Mechanisms for CF_2 radical generation and loss on surfaces in fluorocarbon plasmas

Da Zhang[a)]
Department of Materials Science and Engineering, University of Illinois, 1406 West Green Street, Urbana, Illinois 61801

Mark J. Kushner[b)]
Department of Electrical and Computer Engineering, University of Illinois, 1406 West Green Street, Urbana, Illinois 61801

(Received 20 July 2000; accepted 5 September 2000)

During fluorocarbon plasma etching, plasma-surface reactions result in the surface acting as either a source or sink for reactive species, thereby impacting the properties of the bulk plasma. For example, experiments have shown that surfaces in radio frequency (rf) capacitively coupled discharges can be either sources or sinks of CF_2 depending on, among other properties, the sheath potential. The coupling of rf bulk and surface reactions, and their combined effects on the CF_2 density, were investigated using an integrated plasma equipment and surface kinetics model. While CF_2 sticking on surfaces led to its loss, CF_2 can be generated from surfaces by energetic ion bombardment resulting in sputtering of polymeric films, or neutralization and dissociation of ions. The net effect of a surface for CF_2 production depends on the relative rates of these loss and generation processes. A surface can transform from a net CF_2 sink at low incident ion energies to a CF_2 source at high ion energies because the CF_2 yield by ion–surface interactions typically increases with increasing ion energy. The sensitivity of the model to probabilities of major surface reactions was also investigated. © *2000 American Vacuum Society.* [S0734-2101(00)05106-X]

I. INTRODUCTION

Fluorocarbon plasmas are widely used for silicon and silicon dioxide etching in microelectronics fabrication due to their high rates of etching and selectivity.[1,2] Investigating surface reactions in these plasmas continues to be of interest because, in addition to their direct effects on the etch process, they influence bulk plasma species densities which feed back to etch properties.[3–7] Of particular interest are surface reactions involving CF_2, as CF_2 is a precursor for wafer passivation. Controlling its density is therefore essential to obtaining desirable etch properties. Experiments have demonstrated that surfaces in fluorocarbon plasmas can act as both sinks and sources of CF_2. For example, Fisher, Capps, and Mackie observed that beams of fluorocarbon radicals incident on polymerized surfaces produce additional CF_2.[8] These results imply that reactions of C_xF_y radicals other than CF_2 produced that species at the surface. On the other hand, Sugai, Hikosaka, and Toyota measured a decrease in CF_2 density approaching the substrate in a capacitively coupled radio frequency (rf) plasma reactor indicating that the surface acts as a sink.[9] This discrepancy can be explained by realizing that reactions resulting in the generation and consumption of radicals simultaneously occur at the surface, and it is the relative magnitudes of these processes that determine whether the surface is a net source or sink of CF_2. In fact, a surface in contact with the same plasma chemistry can act as both a source and a sink under different process conditions. These trends have been demonstrated in experiments by Booth *et al.*[5] They showed that in a rf discharge sustained in CF_4, the powered electrode was a CF_2 source at high bias power while the opposite grounded electrode was a sink. The powered electrode turned into a sink when the power was decreased.

In this article, the coupling of surface and plasma reactions is investigated by integrating the Hybrid Plasma Equipment Model (HPEM),[10,11] a plasma simulator, with the Surface Kinetics Model (SKM),[12] which addresses plasma-surface interactions. The consequences of surface reactions in the HPEM are handled using reactive sticking coefficients produced by the SKM. The SKM applies a modified site balance algorithm along reactor surfaces. By using incident plasma fluxes from the HPEM, together with a user defined surface reaction mechanism, the SKM produces the surface coverage of species, incident flux sticking probabilities, and fractional productions of returning species. The system of interest here is a capacitively coupled discharge sustained in CF_4 to enable comparison to Booth's experiments.[5] The surface processes responsible for CF_2 generation and consumption were investigated. We found that CF_2 formation by energetic ion bombardment can exceed CF_2 sticking losses at biased surfaces, making the surfaces a CF_2 source. With decreasing substrate bias, the CF_2 yield by ion-surface interactions decreases due to decreasing ion bombardment energy. The character of the surface (source or sink) is a function of pressure since the ratio of neutral to ion fluxes is pressure dependent. The integrated model is described in Sec. II, followed by a discussion of the surface reaction mechanism for

a)Present address: Motorola Inc., 3501 Ed Bluestein Blvd. MD K20, Austin, TX; electronic mail: r9aabw@email.sps.mot.com
b)Author to whom correspondence should be addressed; electronic mail: mjk@uiuc.edu

a CF_4 plasma in Sec. III. Results for a rf CF_4 discharge are reported and discussed in Sec. IV. Concluding remarks are in Sec. V.

II. DESCRIPTION OF THE INTEGRATED MODEL

The integrated model has been previously described and so will be only briefly discussed here.[12] The HPEM is a two-dimensional simulation consisting of three main modules: Electromagnetic Module (EMM), Electron Energy Transport Module (EETM), and Fluid-chemical Kinetics Module (FKM). Electromagnetic fields and magnetostatic fields are calculated in the EMM and are transferred to the EETM, where electron impact source functions and transport coefficients are derived. Results from the EETM are passed to the FKM, which computes the densities, momentum, and temperatures of plasma species, and solves Poisson's equations for the electrostatic potential. The FKM outputs are then fed back to the EMM and EETM. Converged results are obtained by iterating this process. As capacitively coupled discharges are being discussed here, only the EETM and FKM are employed. The options used for transport are continuity, momentum, and energy equations for all neutral species and ions, continuity (drift diffusion) for bulk electrons, and Monte Carlo for ''beam'' secondary electrons emitted from surfaces.

Surface boundary conditions in the HPEM are handled by a ''flux-in'' and ''flux-out'' algorithm. Species striking a surface are consumed (or stick) with a specified probability. Species then evolve from the surface for a given incident species. Three parameters are used for the plasma-surface interactions; the ''consumption'' coefficient of the incident species, the identify of the evolved species, and the fractional generation rate of the evolved species. These parameters are provided by the SKM.

After accepting incident reactant fluxes from the HPEM, the SKM implements a surface reaction mechanism for surface coverages and layer thickness. The general form of a plasma-surface reaction is

$$A_g + B_s \rightarrow C_s + D_g + E_g, \quad (1)$$

where the subscript g denotes a gas species and the subscript s denotes a surface species. The rate for the ith reaction in the mechanism between gas species A and surface species B and on material m, R_{im}, is

$$R_{im} = k_i \Phi^I_{Am} \theta_{Bm}, \quad (2)$$

where k_i is the reaction probability of the ith reaction, Φ^I_{Am} is the incident flux of plasma species A on material m, and θ_{Bm} is the fractional occupancy of the surface species B. The evolution rates of the coverages of surface species are obtained by summing the rates of reactions generating or consuming the species. The steady state coverages of all surface species are obtained by integrating the coupled rate equations for all surface species using a third-order Runge–Kutta technique. The consumption coefficient for an incident species is then the sum of fractional losses by all reactions removing the species. For an evolved gas species D produced by incident species A on material m, the fractional generation coefficient, f_{ADm}, is then the summation of fractional generation by all reactions of reactant A which produces D. The reaction mechanism allows for deposition of polymer and diffusion of reactive species through the polymer.

For a surface process involving ions (e.g., ion sputtering), the SKM uses an ion energy dependent reaction probability[13]

$$p(E) = p_0 \frac{E^x - E^x_{\mathrm{th}}}{E^x_r - E^x_{\mathrm{th}}}, \quad (3)$$

where $p(E)$ is the reaction probability for an ion with energy E, E_{th} is the threshold energy of the process, E_r is a reference energy, and p_0 is the reaction probability at energy E_r. Experimental data indicate $x = 0.5$ for our ranges of energy and that value was used. In this work, the SKM uses time averaged values for ion energies as is appropriate for low plasma density, thick sheath conditions. First the SKM locates the sheath edge for each surface location. The sheath voltage drop (V_s) at each surface location is obtained by taking the difference between the time averaged voltage at the sheath edge and that at the surface. The energy (E_i) for the ith incident ion is estimated as

$$E_i = \mathrm{Min}\left(1, \frac{\lambda_i}{t_s}\right) \cdot V_s, \quad (4)$$

where λ_i is the mean free path of the ion, and t_s is the sheath thickness.

III. CF_4 PLASMA AND SURFACE REACTION MECHANISMS FOR CF_2 PRODUCTION

Fluorocarbon plasmas are typically used for dielectric etching because of their high etch rates and favorable etch selectivity of SiO_2 over Si.[1,2] The complexity of fluorocarbon plasmas comes from the fact that many types of radicals and ions coexist and contribute differently to surface processes, resulting in simultaneous deposition of polymer passivation layers at surfaces (walls and wafer) during wafer etching.[14,15] The etch rate of Si or SiO_2 is sensitive to the thickness of the polymeric layer which is formed by C_xF_y deposition, usually decreasing with increasing polymer thickness. On the other hand, polymer passivation of the sidewall helps in obtaining anisotropic etch profiles. CF_2 radicals are precursors for both polymer deposition and SiO_2 etching, and so controlling the density of CF_2 is essential to controlling etch properties. Surface reactions have the potential of either depleting or enhancing local CF_2 densities.[4,5,8,9,16]

Experimental evidence of these surface processes is usually obtained by measuring the slope of the CF_2 gas phase density at the surface. A negative slope (decreasing density to the surface) indicates a net flux into the surface, or a sink. A positive slope indicates a source. As a neutral species, CF_2 radicals incident on a surface can chemisorb, thereby decreasing CF_2 density in the plasma region near the surface. One possible source for CF_2 near the surface is the dissociation of large C_xF_y neutrals by energetic ion collisions in the plasma sheath region.[17] In low pressure discharges, the

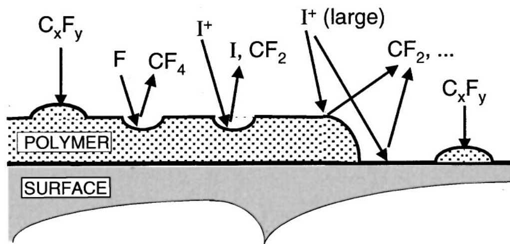

FIG. 1. Schematic of the surface reaction mechanism for a CF_4 discharge without etching. I^+ represents an ion species. Large I^+ species include CF_3^+, $C_2F_4^+$, and $C_2F_5^+$ which can dissociate to form CF_2.

sheath thickness is typically smaller than the mean free paths for ion collisions, and so this source is likely to be small. Reactions *at* the surface are more likely to be sources of CF_2.

In the steady state, the surface is partially or fully covered by polymers deposited from C_xF_y neutrals.[8] Energetic ion sputtering of the polymer layer can generate CF_2 radicals by bond breaking reactions. A net source of CF_2 by this process requires that deposition of the polymer layer be dominantly by C_xF_y radials other than CF_2. Energetic ion bombardment on the surface (bare or polymer passivated), can also produce CF_2 by neutralization of CF_2^+ ions and dissociation of $C_xF_y^+$ ions. This process is, in principle, independent of the polymer coverage of the surface, so it can occur from all surfaces. The net effect of a surface on the production of CF_2 is then dependent on the relative strengths of the consumption and generation of CF_2 by these processes.

A reaction mechanism has been developed for a nonetching surface for a CF_4 plasma to account for these plasma-surface interactions. The mechanism is shown schematically in Fig. 1. The surface reactions are listed in Table I, with reaction probabilities for the base case which will be discussed in Sec. IV. Starting from a bare surface, C_xF_y neutral fluxes (CF, CF_2, C_2F_4, C_2F_5) can stick to the surface to form a polymer layer. C_xF_y fluxes incident on the polymer can also stick. F atoms etch the polymer layer and ion sputtering of the polymer layer erodes the polymer to produce a CF_2 flux from the surface. With the growth of the polymer layer, the polymer consumption by ion sputtering and F atom etching increases, and a steady state polymer coverage is reached where there is no net polymer growth. Large ions (CF_3^+,$C_2F_4^+$,$C_2F_5^+$) bombarding a bare or polymer-covered surface can dissociate to return CF_2 radicals to the plasma. The probabilities of these ion-surface interactions are ion energy dependent as described by Eq. (3).

There is considerable discussion in the literature on the sticking coefficient of CF_2 on surfaces in fluorocarbon plasmas. Goto[18] and Sawin[19] estimated that in the absence of ion activation of surface site, the sticking probability of CF_2 is small ($\sim 10^{-3}$). These results imply that any surface that appears to be a sink for CF_2 requires coincident ion bombardment. There is evidence from the work of Oehrlein[20] that this apparent sticking is preferentially initiated by low energy ion bombardment with activates sticking on other polymers. On the other hand, the work of Booth[5] indicates there

TABLE I. Surface reaction mechanism.

Species definitions:
X_g Gas phase species
W_s Bare surface site
P_s Polymer passivated surface site

Reaction[a,b]	Probability or rate coefficient	Note
$CF_{2g}+W_s \rightarrow P_s$	0.1	c, i
$CF_{2g}+P_s \rightarrow P_s+P_s$	0.1	d, i
$CF_g+W_s \rightarrow P_s$	0.1	c
$CF_g+P_s \rightarrow P_s+P_s$	0.1	d
$C_2F_{4g}+W_s \rightarrow P_s+P_s$	0.03	c
$C_2F_{4g}+P_s \rightarrow P_s+P_s+P_s$	0.03	d
$C_2F_{5g}+W_s \rightarrow P_s+P_s$	0.025	c
$C_2F_{5g}+P_s \rightarrow P_s+P_s+P_s$	0.025	d
$CF_{3g}^+ + W_s \rightarrow CF_{2g}+F_g+W_s$	$p_0=0.45$	e, f, i
$CF_{3g}^+ + P_s \rightarrow CF_{3g}+CF_{2g}+W_s$	$p_0=0.4$	e, g
$CF_{3g}^+ + P_s \rightarrow CF_{2g}+F_g+P_s$	$p_0=0.45$	e, f, i
$C_2F_{4g}^+ + W_s \rightarrow CF_{2g}+CF_{2g}+W_s$	$p_0=0.45$	e, f
$C_2F_{4g}^+ + P_s \rightarrow C_2F_{4g}+CF_{2g}+W_s$	$p_0=0.4$	e, g
$C_2F_{4g}^+ + P_s \rightarrow CF_{2g}+CF_{2g}+P_s$	$p_0=0.45$	e, f
$C_2F_{5g}^+ + W_s \rightarrow CF_{2g}+CF_{3g}+W_s$	$p_0=0.45$	e, f
$C_2F_{5g}^+ + P_s \rightarrow C_2F_{5g}+CF_{2g}+W_s$	$p_0=0.4$	e, g
$C_2F_{5g}^+ + P_s \rightarrow CF_{2g}+CF_{3g}+P_s$	$p_0=0.45$	e, f
$F_g+P_s \rightarrow CF_{4g}+P_s$	0.001	h
$F_g^+ + P_s \rightarrow CF_{2g}+F_g+W_s$	0.3	e, g
$F_{2g}^+ + P_s \rightarrow CF_{2g}+F_{2g}+W_s$	0.35	e, g

[a]Unless otherwise specified, all ions neutralize on all surfaces, returning as their neutral counterparts.
[b]All gas phase species have units of flux ($cm^{-2}\,s^{-1}$). All surface species have units of fractional coverage.
[c]Neutral sticking to bare surface.
[d]Neutral sticking to polymer passivated surface.
[e]See Eq. (3). $E_r=150$ eV, $E_{th}=5$ eV.
[f]Ion dissociation at surface.
[g]Ion sputtering of polymer passivated surface.
[h]F atom etching of the polymer layer.
[i]Base case value. See text for sensitivity analysis.

is net sticking of CF_2 to surfaces when power is removed from his reactor. Granted there could be a small flux of low energy ions which continue to initiate sticking sites late into the afterglow, though this is unlikely. Given these contradictory results, we choose to express CF_2 sticking in terms of an effective coefficient which may include some degree of ion activation.

The gas phase chemistry used in the simulation is summarized in Table II. The formation of CF_2 radicals mainly comes from electron impact dissociation of CF_4, CF_3, and C_2F_4. Five positive ion species are produced: CF_3^+, $C_2F_4^+$, $C_2F_5^+$, F_2^+, and F^+. For these conditions, CF_3^+ is the dominant ion.

IV. CF_2 PRODUCTION AND LOSS IN A rf CF_4 DISCHARGE

The capacitively coupled rf discharge used in this study is patterned after Booth *et al.*[5] and is shown schematically in Fig. 2. The reactor is cylindrical with a radius of 14.5 cm. The radius of the lower electrode (3 cm from the reactor bottom) is 5.5 cm, and the radius of the upper electrode, which is 3.3 cm above the lower electrode, is 14 cm. A rf bias at 13.56 MHz is applied to the lower electrode, which is

TABLE II. CF_4 gas phase reaction mechanism.[a]

Species: CF_4, CF_3, CF_3^+, CF_3^-, CF_2, CF, F, F^+, F^-, F_2, F_2^+, C_2F_6, C_2F_5, $C_2F_5^+$, C_2F_4, $C_2F_4^+$, C_2F_3, *e*.

Reaction	Rate coefficient[b]	Reference
$e+CF_4 \rightarrow CF_3+F^-$	c	22
$e+CF_4 \rightarrow CF_3^-+F$	c	22
$e+CF_4 \rightarrow CF_3+F+e$	c	22
$e+CF_4 \rightarrow CF_3^++F+e+e$	c	22
$e+CF_4 \rightarrow CF_2+F+F+e$	c	22
$e+CF_3 \rightarrow CF_2+F+e$	c	22[d]
$e+CF_3 \rightarrow CF_2+F^-$	c	22[d]
$e+CF_2 \rightarrow CF+F+e$	c	22[d]
$e+CF_2 \rightarrow CF+F^-$	c	22[d]
$e+C_2F_6 \rightarrow CF_3^++CF_3+e+e$	c	23
$e+C_2F_6 \rightarrow CF_3+CF_3^-$	c	23
$e+C_2F_6 \rightarrow C_2F_5+F^-$	c	23
$e+C_2F_6 \rightarrow CF_3+CF_3+e$	c	23
$e+C_2F_4 \rightarrow CF_2+CF_2+e$	c	23[e]
$e+C_2F_4 \rightarrow C_2F_4^++e+e$	c	23[e]
$e+C_2F_4 \rightarrow F^-+C_2F_3$	c	23
$e+F_2 \rightarrow F^-+F$	c	24[f]
$e+F_2 \rightarrow F+F+e$	c	24[f]
$e+F_2 \rightarrow F_2^++e+e$	c	24[f]
$e+F \rightarrow F^++e+e$	c	25
$e+CF_3^+ \rightarrow CF_2+F$	2.0×10^{-8}	24[f]
$e+C_2F_5^+ \rightarrow CF_3+CF_2$	2.0×10^{-8}	24[f]
$e+C_2F_4^+ \rightarrow CF_2+CF_2$	2.0×10^{-8}	24[f]
$e+F_2^+ \rightarrow F+F$	2.0×10^{-8}	24[f]
$CF_3^++CF_3 \rightarrow CF_3^++CF_3$	1.0×10^{-9}	26
$CF_3^++C_2F_6 \rightarrow C_2F_5^++CF_4$	3.50×10^{-11}	26
$C_2F_5^++C_2F_5 \rightarrow C_2F_5^++C_2F_5$	1.0×10^{-9}	26
$C_2F_4^++C_2F_4 \rightarrow C_2F_4^++C_2F_4$	1.0×10^{-9}	26
$F^-+CF_3^+ \rightarrow F+CF_3$	1.0×10^{-7}	27
$F^-+C_2F_4^+ \rightarrow F+C_2F_4$	1.0×10^{-7}	27
$F^-+C_2F_5^+ \rightarrow F+C_2F_5$	1.0×10^{-7}	27
$F^-+F_2^+ \rightarrow F+F_2$	1.0×10^{-7}	27
$F^-+F^+ \rightarrow F+F$	1.0×10^{-7}	27
$CF_3^-+CF_3^+ \rightarrow CF_3+CF_3$	1.0×10^{-7}	27
$CF_3^-+C_2F_4^+ \rightarrow CF_3+C_2F_4$	1.0×10^{-7}	27
$CF_3^-+C_2F_5^+ \rightarrow CF_3+C_2F_5$	1.0×10^{-7}	27
$CF_3^-+F_2^+ \rightarrow CF_3+F_2$	1.0×10^{-7}	27
$CF_3^-+F^+ \rightarrow CF_3+F$	1.0×10^{-7}	27
$CF_3^-+F \rightarrow CF_3+F^-$	5.0×10^{-8}	27
$F+F+M \rightarrow F_2+M$	6.77×10^{-28}	28
$F+C_2F_4 \rightarrow CF_3+CF_2$	4.0×10^{-11}	29
$F+C_2F_5 \rightarrow CF_3+CF_3$	1.0×10^{-11}	29
$F+C_2F_3 \rightarrow C_2F_4$	1.0×10^{-12}	30
$F+CF_3 \rightarrow CF_4$	1.30×10^{-11}	31
$F+CF_2 \rightarrow CF_3$	8.40×10^{-15}	29
$F_2+CF_2 \rightarrow CF_3+F$	4.56×10^{-13}	30
$F_2+CF_3 \rightarrow CF_4+F$	1.88×10^{-14}	30
$CF_3+CF_3 \rightarrow C_2F_6$	7.67×10^{-12}	30
$CF_2+CF_2 \rightarrow C_2F_4$	5.0×10^{-14}	30
$CF_2+CF_3 \rightarrow C_2F_5$	8.26×10^{-13}	30

[a]Only reactions directly affecting species densities are shown here. Additional electron impact collisions (e.g., momentum transfer, vibrational excitation) are included in the EETM.
[b]Rate coefficients have units $cm^3\,s^{-1}$ unless noted otherwise.
[c]Computed using the electron energy distribution and electron impact cross section from cited reference.
[d]Estimated by analogy to CF_4.
[e]Estimated by analogy to C_2F_6.
[f]Estimated. See cited reference for similar reaction.

surrounded by a dark space shield. The top and side walls of the reactor are grounded. Pure CF_4 gas is supplied through the top shower head and is pumped from the bottom outlet. No wafer is used in the reactor. The base case conditions are

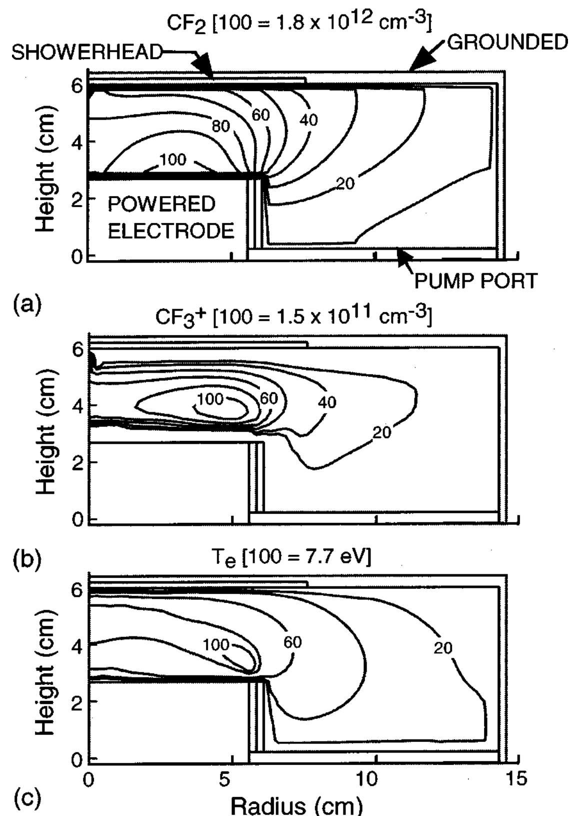

FIG. 2. Densities of (a) CF_2 and (b) CF_3^+ and (c) electron temperature in the rf reactor for the base case conditions (50 mTorr, 250 V bias, 30 sccm, surface reaction probabilities as shown in Table I). The labels on the contour lines denote the percentage of the value shown at the top of each figure. Electric field enhancement produces peak values near the edge of the electrodes.

CF_4 at 50 mTorr, 30 sccm gas flow rate, 250 V rf bias amplitude, and surface reaction probabilities as shown in Table I.

CF_2 and CF_3^+ densities for the base case are shown in Fig. 2. The two densities peak close to the edge of the powered electrode due to electric field enhancement near the corner of the electrode. As a result the electron temperature in that region is also higher, as shown in Fig. 2(c). For this case, the CF_2 density is highest near the powered surface, implying surface reactions there produce a net source of CF_2.

The axial CF_2 densities at a radius of 3.5 cm are shown in Fig. 3(a) for substrate biases of 30–250 V. On the grounded upper electrode, CF_2 densities decrease from the bulk plasma to the surface for all biases, indicating a sink. On the powered lower electrode, the CF_2 density is maximum at the surface for high bias, indicating a source. With decreasing substrate bias, the slope of axial CF_2 density decreases and eventually is negative at sufficiently low biases, indicating a sink. For example, the CF_2 density at 30 V bias is shown in Fig. 3(b), and shows a peak in the density in the bulk plasma.

The variation of substrate bias has two major effects on the CF_2 density. First the power deposition increases with increasing bias, resulting in more dissociation and more production of CF_2 in the gas phase. The increase in power pro-

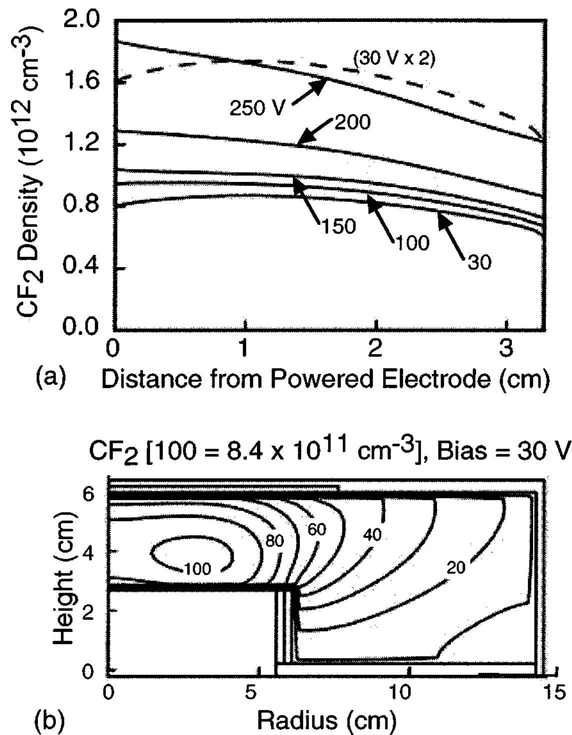

FIG. 3. CF_2 for different biases. (a) Densities at $r=3.5$ cm as a function of height. (b) CF_2 density for 30 V bias. All cases are at 50 mTorr and 30 sccm. Increasing the bias increases the source of CF_2 at the powered electrode.

duces increases of CF_2 and ion densities in approximately the same proportion. As a result the relative strengths of CF_2 loss and generation at the surface are unchanged. The second effect of varying bias is the change in plasma sheath voltages at surfaces. At 13.56 MHz, the time averaged sheath voltage drop increases with increasing bias amplitude, thereby increasing the incident ion energies. Since sputter yields increase with energy, thereby increasing CF_2 production, the spatial distribution of CF_2 can be a function of bias.

The sheath voltage drops as a function of substrate bias on both the powered and grounded electrode at a radius of 3.5 cm (Fig. 4). Due to the unequal areas of the grounded electrode and the biased electrode, there is a large dc bias on the powered electrode. This increases the sheath voltage drop at the powered electrode relative to that at the grounded electrode. For all biases from 30 to 250 V, the sheath voltages at the grounded electrode are low and near the threshold energies of ion sputtering or ion dissociation, having a maximum of only ≈25 V. This leads to small rates of ion-surface reactions, and so CF_2 generation rates are also small. For such conditions, the CF_2 sticking at the grounded surface dominates and the net effect of the grounded surface is as a sink for CF_2.

At the powered electrode, when the bias is 30 V the resulting average sheath potential is only ≈20 V, so the ion bombardment energy is low, making the surface a sink for CF_2. As the bias is increased to 100 V, the average sheath potential increases to 78 V, which is large enough to make the CF_2 generation rate by ion bombardment to be comparable with the rate of CF_2 sticking. As a result the axial CF_2 density profile is nearly flat at the surface. With a further increase of the substrate bias, CF_2 generation rate exceeds its sticking loss, and so the surface acts as a net source for CF_2. The CF_2 density then increases from the plasma region to the surface. The slope of the axial CF_2 density increases with bias due to the increasing CF_2 yield by ion bombardment.

The model results were validated by comparing to the experimental data of Booth *et al.*[5] To compare to Booth's transient experiments, we performed simulations at 100 W rf bias until the plasma reached a steady state. The source power was then turned off and the simulation was continued for several ms. Simulated and experimental CF_2 axial densities at 100 W and after power was turned off are shown in

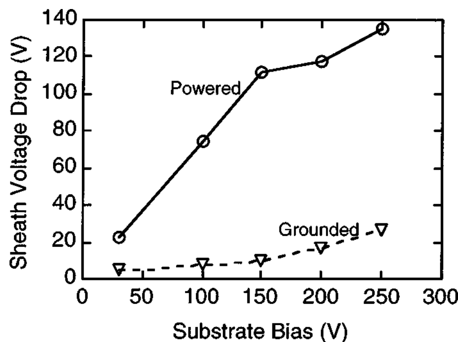

FIG. 4. Time averaged sheath voltage drop as a function of the substrate bias at the powered and grounded surfaces. The sheath at the grounded electrode remains sufficiently low that the surface always appears to be a sink for CF_2.

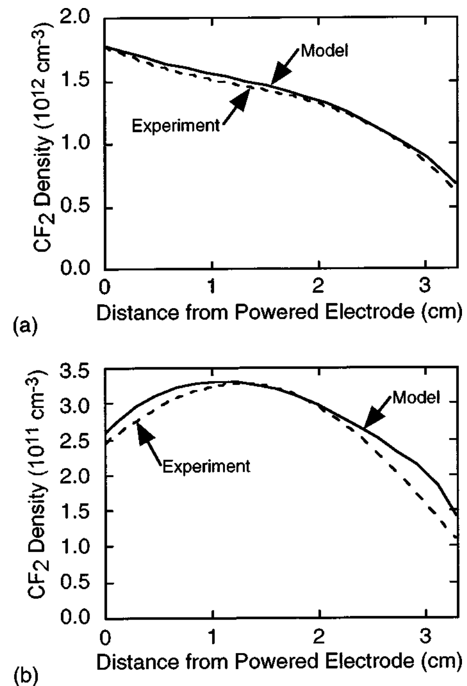

FIG. 5. Axial CF_2 densities at (a) 100 W rf power and (b) after the power is turned off. The solid lines are simulation results and the dashed lines are experimental results from Booth (see Ref. 5).

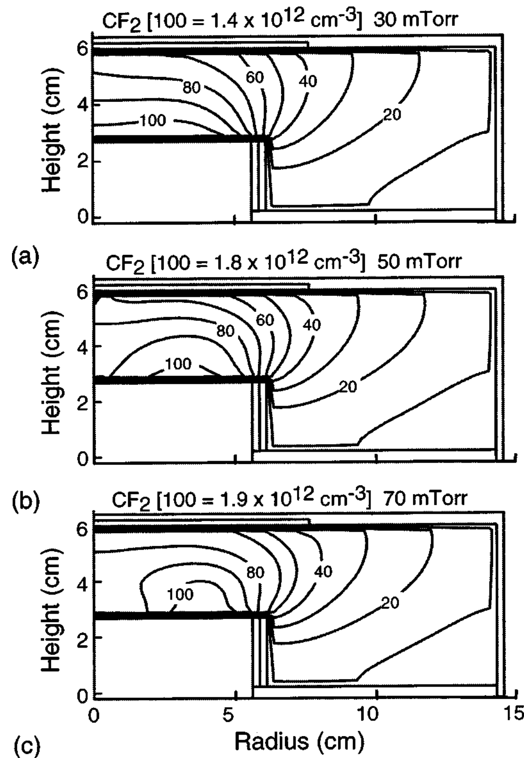

FIG. 6. CF_2 density at (a) 30, (b) 50, (c) 70 mTorr. All cases are at 250 V bias and 30 sccm. The labels on the contour lines denote the percentage of the value shown at the top of each figure. Increasing pressure localizes sources closer to the power electrode.

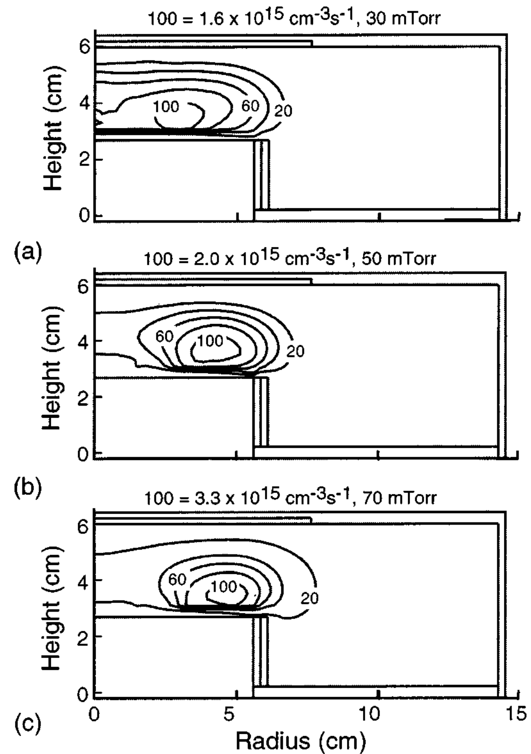

FIG. 7. CF_2 source functions at (a) 30, (b) 50, (c) 70 mTorr. The conditions are the same as for Fig. 6. Increasing pressure shifts the maximum in the source to larger radius.

Fig. 5. When the power is on, CF_2 densities decrease from the powered lower electrode to the grounded upper electrode for both simulation and experiments, indicating a source of CF_2 at the powered electrode and a sink at the grounded electrode. When the power is turned off, the initially powered electrode transitions into a CF_2 sink, and so CF_2 densities decrease at the lower electrode as well as at the upper electrode. The simulation reproduced the experimental trends.

Gas pressure is an important process parameter due to its direct effect on the source neutral density, and its influence on plasma transports and species densities. We simulated discharges at 30, 50, and 70 mTorr while keeping other parameters the same as those in the base case. The resulting CF_2 densities and CF_2 source functions are shown in Figs. 6 and 7, respectively. The peak CF_2 density increases with pressure due to both a larger and more confined source and a lower rate of diffusion. At high pressure (70 mTorr), the peak CF_2 source occurs at a larger radius due to electric field enhancement and localized power deposition. As the pressure decreases, the electron energy relaxation length increases, and diffusion rates increase, resulting in the peak CF_2 area expanding to the reactor center. At all pressures the CF_2 densities are maximum at the surface of the powered electrode, implying a net CF_2 source there resulting from the high bias of 250 V. Axial CF_2 densities at a radius of 3.5 cm for 30, 50, and 70 mTorr are shown in Fig. 8(a). The powered electrode is a net source of CF_2 in all cases. The strength of the source is indicated by the slope of the density at the surface. At 30 mTorr, the slope is the steepest, becoming shallower with increasing pressure.

Pressure can impact the plasma floating potential through the electron temperature. Lower pressures imply higher electron temperatures and larger floating potentials. Since the floating potential is small compared with the applied bias (250 V), and since the sheath is largely noncollisional at these pressures, the majority of the plasma sheath potential comes from the bias. The influence of pressure on the incident ion energy is therefore weak. The ratio of ion to neutral fluxes to the surface, however, can change significantly with pressure. For example, after being normalized to the value at 30 mTorr, the ratios of ion to neutral fluxes at different pressures are shown in Fig. 8(b). The ratio decreases with increasing pressure which means the CF_2 generation by ion bombardment decreases with increasing pressure relative to CF_2 sticking. Therefore the surface progressively appears as a sink, as indicated by the slopes in Fig. 8(b).

CF_2 generation comes from ion sputtering and ion dissociation, and so the probabilities of these processes determine the strength of the CF_2 source. Ion sputtering of CF_2, unlike ion dissociation, also depends on the polymer coverage. Thus far, we used $p_0=0.45$ for ion dissociation and $p_0=0.4$ for ion sputtering. [The final reaction probability is obtained from Eq. (3). For both processes $E_r=150\,\mathrm{eV}$ and $E_{\mathrm{th}}=5\,\mathrm{eV}$ were used.] The polymer coverage for the base case is close to unity at ≈ 0.9. So the relative contributions of ion sputtering and ion dissociation to CF_2 generation are

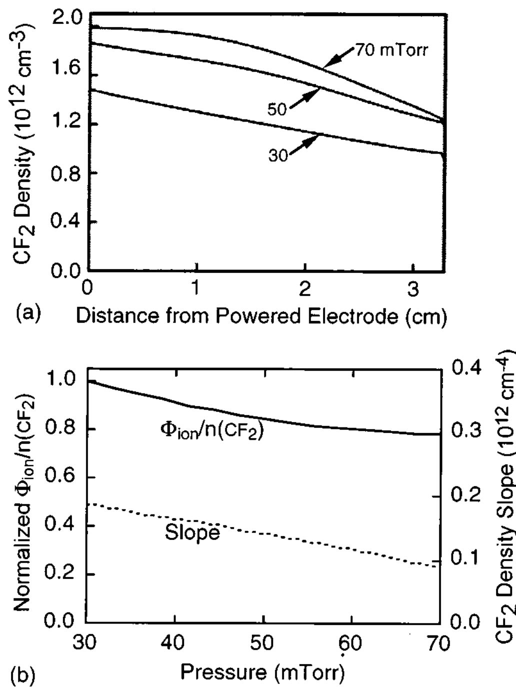

FIG. 8. CF_2 properties as a function of pressure. (a) Axial CF_2 densities at $r=3.5$ cm for 30, 50, and 70 mTorr. (b) The ratio of ion flux to CF_2 density, and the slope of the CF_2 density at the powered electrode of $r=3.5$ cm as a function of pressure. The values of the ratios of ion flux to CF_2 density are normalized to that at 30 mTorr. The increase in pressure reduces the ion flux relative to the neutral flux, and as a result weakens the net source of CF_2, as indicated by the reduction in slope.

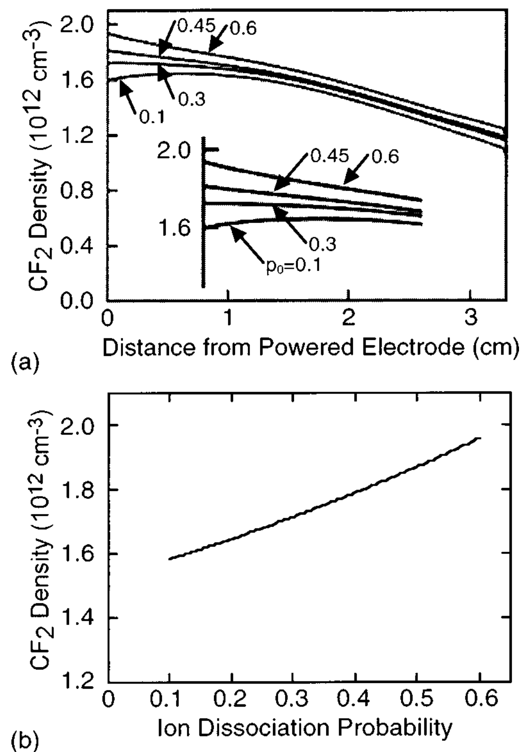

FIG. 9. CF_2 properties as a function of ion dissociation probability. (a) Axial CF_2 density at $r=3.5$ cm for different ion dissociation probabilities. All cases are at 50 mTorr, 250 V bias, and 30 sccm. (b) The CF_2 density at $z=3$ cm as a function of the ion dissociation probability at the surface. Increasing the ion dissociation probability increases the net source of CF_2.

estimated to be ≈0.36:0.45 or 4:5. Given the fact that some surface reaction probabilities change with process conditions (e.g., CF_2 sticking coefficients being a function of surface temperature[7]), and considering the uncertainty in selecting coefficients for the model, it is valuable to investigate the sensitivity of the simulation to the selection of coefficients. Axial CF_2 densities at a radius of 3.5 cm for different p_0 for ion dissociation are shown in Fig. 9(a). The CF_2 density at the powered electrode as a function of p_0 is plotted in Fig. 9(b). Other parameters are the same as in the base case. For small dissociation probabilities (0.1,0.3), the powered surface acts as a sink for CF_2. CF_2 sources are dominated by sputtering, which is insufficient to produce a net source. When the dissociation probability is large enough, the powered surface becomes a CF_2 source. However, on the grounded side, since the CF_2 generation by ion bombardment is negligible in all cases, the ion dissociation probability has little influence on the slope of the CF_2 density at that electrode.

The sensitivity of the model to the effective CF_2 sticking coefficient, α, was also investigated. The axial CF_2 densities at a radius of 3.5 cm are shown in Fig. 10(a) for CF_2 sticking coefficients from 0.05 to 0.6 (the base case value is 0.1). Large sticking coefficients ($\alpha \geqslant 0.2$) result in a net CF_2 loss at the surface, so the CF_2 density decreases with increasing sticking coefficient at both powered and grounded electrodes. As the sticking coefficient drops to $\alpha=0.1$, the CF_2 generation rate exceeds the loss rate at the powered surface, and so the CF_2 density increases from the plasma region to the surface. At the grounded electrode, the CF_2 sticking always dominates as there is little effect by ion-surface reactions. The CF_2 density therefore decreases towards the surface in all cases. Sticking coefficients of $\alpha<0.1$ are typically required for surfaces to be net sources for these biases. The CF_2 densities as a function of sticking coefficients at the powered surface (height=3.0 cm) and in the bulk region (height=3.8 cm) are shown in Fig. 10(b). The density drops with increasing sticking coefficient at both locations. The density at the surface drops more rapidly due to the proximity of CF_2 consuming reactions.

The production of CF_2 is sensitive to both p_0, the ion dissociation probability, and α, the CF_2 sticking coefficient. The combined effects of p_0 and α on the slope of the CF_2 density approaching the surface were investigated statistically using a design of experiment method, implemented in the commercial software, ECHIP.[21] The results are shown in Fig. 10(c). The slopes (S) are labeled on the response lines with a unit of $10^{12}\,cm^{-4}$. The S=0.0 line defines the boundary between the source and sink regions, with S>0 indicating a source and S<0 a sink. S is more sensitive to α than to p_0, since the neutral flux is larger than the ion flux at the surface. The general trend is that increasing p_0 and decreasing α produce a surface source of CF_2.

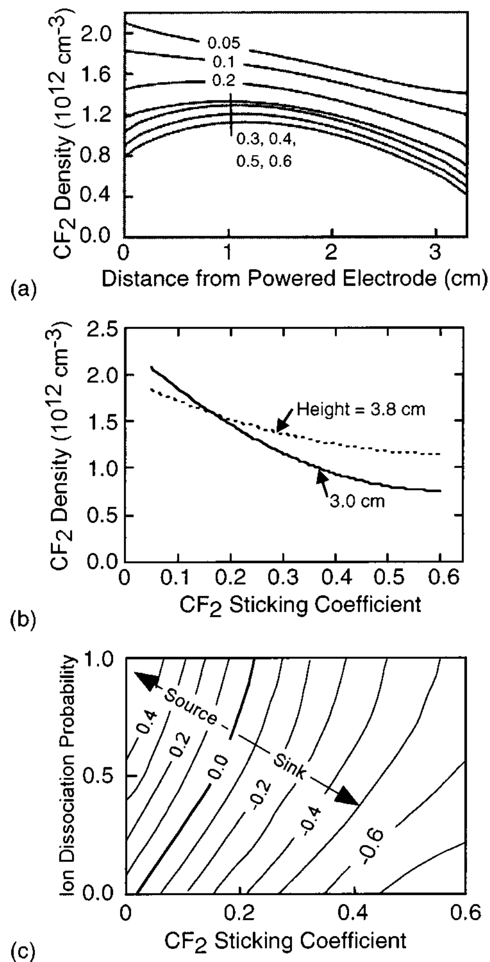

FIG. 10. CF_2 properties as a function of sticking probability. (a) Axial CF_2 density at $r=3.5$ cm for different CF_2 sticking coefficients. All cases are at 50 mTorr, 250 V bias, and 30 sccm. (b) The CF_2 densities at $z=3$ cm and $z=3.8$ cm as function of the sticking coefficients. (c) The slope of the CF_2 density approaching the powered surface as a function of the CF_2 sticking coefficient and the ion dissociation probability. The slopes are labeled on the response lines with a unit of 10^{12} cm^{-4}.

V. CONCLUDING REMARKS

An integrated surface kinetics and plasma equipment model was used to investigate the effect of ion and neutral reactions at the surface of a rf CF_4 discharge on the CF_2 density. CF_2 sticking is a loss at the surface, while ion sputtering of deposited polymer layers and ion dissociation can generate CF_2. The net effect of the surface then depends on the relative rates of the CF_2 loss and ion generation. The reaction probabilities of ion-surface reactions increase with increasing incident ion energy, and so a surface can transform from a net CF_2 sink at low bias to a net CF_2 source at high bias. The ratios of ion flux to CF_2 density near a surface are a function of pressure, and this leads to different CF_2 density profiles near the surface at different pressures. The sensitivities of the model on rate coefficients were analyzed. Large ion dissociation probabilities and small CF_2 sticking coefficients produce a CF_2 source at the surface.

ACKNOWLEDGMENTS

This work was supported by the Semiconductor Research Corporation, Applied Materials, LAM Research Corporation, DARPA/AFOSR, and the National Science Foundation (CTS99-74962).

[1]N. R. Rueger, M. F. Doemling, M. Schaepkens, J. J. Beulens, T. E. F. M. Standaert, and G. S. Oehrlein, J. Vac. Sci. Technol. A **17**, 2492 (1999).
[2]T. E. F. M. Standaert, M. Schaepkens, N. R. Rueger, P. G. M. Sebel, G. S. Oehrlein, and J. M. Cook, J. Vac. Sci. Technol. A **16**, 239 (1998).
[3]J. A. O'Neil and J. Singh, J. Appl. Phys. **77**, 497 (1995).
[4]G. M. W. Kroesen, H. Lee, H. Moriguchi, H. Motomura, T. Shirafuji, and K. Tachibana, J. Vac. Sci. Technol. A **16**, 225 (1998).
[5]J. P. Booth, G. Cunge, P. Chabert, and N. Sadeghi, J. Appl. Phys. **85**, 3097 (1999).
[6]G. Cunge and J. P. Booth, J. Appl. Phys. **85**, 3952 (1999).
[7]M. Schaepkens, R. C. M. Bosch, T. E. F. M. Standaert, and G. S. Oehrlein, J. Vac. Sci. Technol. A **16**, 2099 (1998).
[8]N. E. Capps, N. M. Mackie, and E. R. Fisher, J. Appl. Phys. **84**, 4376 (1998).
[9]Y. Hikosaka, H. Toyota, and H. Sugai, Jpn. J. Appl. Phys., Part 2 **32**, L353 (1993).
[10]S. Rauf and M. J. Kushner, J. Appl. Phys. **83**, 5087 (1998).
[11]M. J. Grapperhaus and M. J. Kushner, J. Appl. Phys. **81**, 569 (1997).
[12]D. Zhang and M. J. Kushner, J. Appl. Phys. **87**, 1060 (2000).
[13]C. F. Adams and D. B. Graves, J. Appl. Phys. **86**, 2263 (1999).
[14]A. J. Bariya, C. W. Frank, and J. P. McVittie, J. Electrochem. Soc. **137**, 2575 (1990).
[15]S. Samukawa and S. Furuoya, Jpn. J. Appl. Phys., Part 2 **32**, L1289 (1993).
[16]C. Suzuki, K. Sasaki, and K. Kadota, J. Vac. Sci. Technol. A **16**, 2222 (1998).
[17]M. Haverlay, W. W. Stoffels, E. Stoffels, G. M. W. Kroesen, and F. J. de Hoog, J. Vac. Sci. Technol. A **14**, 384 (1996).
[18]K. Teii, M. Hori, and T. Goto, J. Appl. Phys. **87**, 7185 (2000).
[19]D. C. Gray, I. Tepermeister, and H. H. Sawin, Proceedings of the 2nd International Conference on Reactive Plasmas, Yokohama, Japan, 1994 (unpublished).
[20]M. Shaepkens, G. S. Oehrlein, and J. M. Cook, J. Vac. Sci. Technol. B **18**, 848 (2000).
[21]ECHIP, Inc., http://www.echip.com
[22]R. A. Bonham, Jpn. J. Appl. Phys., Part 1 **33**, 4157 (1994).
[23]M. Hayashi, in *Gaseous Dielectrics V*, edited by L. G. Christophorou and D. W. Bouldin (Pergamon, New York, 1987).
[24]M. Hayashi and T. Nimura, J. Appl. Phys. **54**, 4879 (1983).
[25]W. L. Morgan (private communication).
[26]E. Fisher, M. E. Weber, and P. B. Armentrout, J. Chem. Phys. **76**, 4932 (1982).
[27]R. E. Olson, J. R. Peterson, and J. Moseley, J. Chem. Phys. **53**, 3391 (1971).
[28]E. L. Duman, N. P. Tishchenko, and I. P. Shmatov, Dokl. Phys. Chem. **295**, 5 (1987).
[29]I. C. Plumb and K. R. Ryan, Plasma Chem. Plasma Process. **6**, 205 (1986).
[30]D. R. F. Burgess, Jr., M. R. Zachariah, W. Tsang, and P. R. Westmoreland, Prog. Energy Combust. Sci. **21**, 453 (1996).
[31]D. R. F. Burgess, Jr., National Institute of Standards and Technology (private communication).